1521-009X/49/10/856–868$35.00
DRUG METABOLISM AND DISPOSITION

https://doi.org/10.1124/dmd.121.000508
Drug Metab Dispos 49:856–868, September 2021

Infigratinib Is a Reversible Inhibitor and Mechanism-Based Inactivator of Cytochrome P450 3A4[S]

Lloyd Wei Tat Tang, Jian Wei Teng, Ravi Kumar Verma, Siew Kwan Koh, Lei Zhou, Mei Lin Go, Hao Fan, and Eric Chun Yong Chan

Department of Pharmacy, Faculty of Science (L.W.T.T., J.W.T, M.L.G., E.C.Y.C.) and Department of Ophthalmology, Yong Loo Lin School of Medicine (L.Z.), National University of Singapore, Singapore; Bioinformatics Institute, Agency for Science, Technology and Research, Singapore (R.K.V., H.F.); Singapore Eye Research Institute, Singapore (S.K.K., L.Z.); and Ophthalmology and Visual Sciences Academia Clinical Program, Duke-National University of Singapore Medical School, Singapore (L.Z.)

Received April 19, 2021; accepted July 08, 2021

ABSTRACT

Infigratinib (INF) is a promising selective inhibitor of fibroblast growth factor receptors 1–3 that has recently been accorded both orphan drug designation and priority review status by the US Food and Drug Administration for the treatment of advanced cholangiocarcinoma. Its propensity to undergo bioactivation to electrophilic species was recently expounded upon. However, other than causing aberrant idiosyncratic toxicities, these reactive intermediates may elicit mechanism-based inactivation of cytochrome P450 enzymes. In this study, we investigated the interactions between INF and the most abundant hepatic CYP3A. Our findings revealed that, apart from being a potent noncompetitive reversible inhibitor of CYP3A4, INF inactivated CYP3A4 in a time-, concentration- and NADPH-dependent manner with inactivator concentration at half-maximum inactivation rate constant, maximum inactivation rate constant, and partition ratio of 4.17 μM, 0.068 minute^{-1}, and 41, respectively, when rivaroxaban was employed as the probe substrate. Coincubation with testosterone (alternative CYP3A substrate) or ketoconazole (direct CYP3A inhibitor) attenuated the rate of inactivation, whereas the inclusion of glutathione and catalase did not confer such protection. The lack of enzyme activity recovery after dialysis for 4 hours and oxidation with potassium ferricyanide, coupled with the absence of the characteristic Soret peak signature collectively substantiated that inactivation of CYP3A4 by INF was not mediated by the formation of quasi-irreversible metabolite-intermediate complexes but rather through irreversible covalent adduction to the prosthetic heme and/or apoprotein. Finally, glutathione trapping and high-resolution mass spectrometry experimental results unraveled two plausible bioactivation mechanisms of INF arising from the generation of a *p*-benzoquinonediimine and epoxide reactive intermediate.

SIGNIFICANCE STATEMENT

The potential of INF to cause MBI of CYP3A4 was unknown. This study reports the reversible noncompetitive inhibition and irreversible covalent MBI of CYP3A4 by INF and proposes two potential bioactivation pathways implicating *p*-benzoquinonediimine and epoxide reactive intermediates, following which a unique covalent docking methodology was harnessed to elucidate the structural and molecular determinants underscoring its inactivation. Findings from this study lay the groundwork for future investigation of clinically relevant drug-drug interactions between INF and concomitant substrates of CYP3A4.

Introduction

Fibroblast growth factor receptor (FGFR) genomic aberrations have been reported in numerous cancers and are intricately linked to tumor cell proliferation, survival, and migration (Haugsten et al., 2010; Turner and Grose, 2010). Consequently, pharmacological ablation of FGFR signaling pathways is rapidly gaining prominence as a promising modality in cancer therapeutics (Dienstmann et al., 2014). To date, two FGFR-selective inhibitors (i.e., erdafitinib and pemigatinib) have already garnered global regulatory approval, and a fleet of upcoming FGFR inhibitors in various phases of drug development have shown encouraging preclinical and clinical responses (Chae et al., 2017; Markham, 2019; Hoy, 2020). Infigratinib (INF), formerly designated as

This work was supported by the Agency for Science, Technology and Research (A*STAR) Industry Alignment Fund – Pre-Positioning (IAF-PP) [Grant H18/01/a0/C14] and the Joseph Lim Boon Tiong Urology Cancer Research Initiative [Grant R-148-000-302-720] to E.C.Y.C. L.W.T.T. is supported by the National University of Singapore (NUS) President's Graduate Fellowship (PGF).

The authors declare that they have no conflicts of interest with the contents of this article.

http://dx.doi.org/10.1124/dmd.121.000508.

[S] This article has supplemental material available at dmd.aspetjournals.org.

ABBREVIATIONS: BEH, ethylene bridged hybrid; CUR, curtain gas; DDI, drug-drug interaction; EPI, enhanced product ion; ESI, electrospray ionization; FDA, US Food and Drug Administration; FGFR, fibroblast growth factor receptor; GSH, glutathione; G6P, glucose-6-phosphate; G6PDH, glucose-6-phosphate dehydrogenase; INF, infigratinib; K_i, reversible inhibition constant; K_I, inactivator concentration at half-maximum inactivation rate constant; k_{inact}, maximum inactivation rate constant; K_m, Michaelis constant; k_{obs}, observed first-order rate constant of inactivation; LC/MS/MS, liquid chromatography tandem mass spectrometry; MBI, mechanism-based inactivation; MI, complex metabolite-intermediate complex; MS/MS, tandem mass spectrometry; NL, neutral loss; OBS, orthosteric binding site; P450, cytochrome P450; PIS, precursor ion scan; QTOF, quadrupole time-of-flight; rhCYP3A4, recombinant human cytochrome P450 3A4; rhCYP3A5, recombinant human cytochrome P450 3A5; ROS, reactive oxygen species; $t_{1/2}$, half-life.

BGJ398 (Fig. 1), is a highly potent and selective ATP-competitive inhibitor of FGFR1–3 that is currently under clinical investigation for several FGFR-driven cancers (Javle et al., 2018; Botrus et al., 2021). Notably, it has been accorded both orphan drug designation and priority review status by the US Food and Drug Administration (FDA) for the treatment of advanced cholangiocarcinoma, a rare malignancy plagued with an extremely poor prognosis and limited therapeutic options (Mosconi et al., 2009).

However, a recent study has identified several putative reactive metabolites of INF that are proposed to have arisen from cytochrome P450 enzyme (P450)-mediated metabolic activation of its *N*-ethyl piperazine and dimethoxybenzene ring moieties (Al-Shakliah et al., 2020). In that regard, the P450s are a ubiquitous family of hemoproteins that serve as one of the major drivers of xenobiotic oxidative metabolism in the human body (Guengerich, 2001; Zanger and Schwab, 2013). It is estimated that just six P450 isoforms contribute to the metabolism of >80% of all marketed drugs (Zanger et al., 2008), thereby entrenching their importance in drug metabolism. Inadvertently, because of its wide substrate specificities and diversity of reactions that P450s can catalyze, they may also be responsible for metabolic activation of drugs (Guengerich, 2001). These group of reactions are collectively termed as bioactivation, and they result in the generation of electrophilic, reactive metabolites that, when liberated, can covalently alkylate to nucleophilic centers on biologic macromolecules or generate reactive oxygen species (ROS) leading to oxidative stress (Stephens et al., 2014). These deleterious cellular and molecular perturbations can collectively result in idiosyncratic organ-related toxicities. Inasmuch as the liver is the main site for drug metabolism, it is frequently implicated in bioactivation-mediated toxicities.

Apart from the overt toxicological implications of P450-mediated bioactivation, the reactive intermediate generated can be sequestered within the enzyme and cause mechanism-based inactivation (MBI) via covalent adduction to nucleophilic residues within the apoprotein and/or heme porphyrin ring or through coordination with the heme catalytic iron (Ho et al., 2015). As the loss of enzymatic activity is irreversible and persists in vivo even after the inactivator has been systemically cleared from the body and is only restored upon biosynthesis of new enzymes, the extent of endobiotic-xenobiotic interactions and/or drug-drug interactions (DDI) tends to be more profound than with a reversible inhibitor (Bjornsson et al., 2003). Furthermore, MBI of P450 could also lead to autoinhibition of hepatic elimination, time-dependent and/or nonlinear pharmacokinetics. Finally, covalent modification of the P450 protein may constitute neoantigens and trigger adaptive immune responses which can culminate in immune-mediated toxicities (Masubuchi and Horie, 2007). Because of its manifold ramifications in pharmacology and toxicology, it becomes clinically important to discern whether a drug elicits MBI of P450.

At this outset, a drug can be characterized as an archetypal MBI of P450 if it exhibits the following features: time- and cofactor-dependency of inactivation, saturable kinetics of inactivation, protection against inactivation by a competing substrate, lack of protection by exogenous nucleophiles or scavengers of ROS, irreversibility of inactivation, and a 1:1 binding stoichiometry (Silverman, 1995). Although the potential for INF to undergo bioactivation has been previously demonstrated, it should be noted that these conclusions were drawn from experiments conducted in rat liver microsomes. Consequently, its propensity to undergo bioactivation and elicit MBI of human P450 remains obfuscated. However, there have been multiple reports of INF accumulation at therapeutic doses in phase I studies (Nogova et al., 2017; Kelly et al., 2019). These clinical observations provided the impetus for us to investigate whether INF could elicit any MBI against CYP3A (i.e., CYP3A4/5), which are known to play a major role in its metabolism (Reyes et al., 2020).

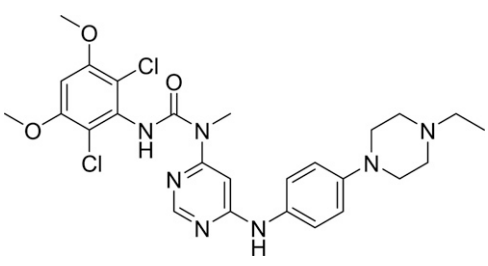

Fig. 1. Chemical structure of infigratinib (INF).

In this study, we revealed for the first time that INF is a potent noncompetitive reversible inhibitor and MBI of CYP3A4. Thereafter, we further demonstrated that INF fulfills all the established criteria for an irreversible MBI and trapped the reactive intermediate responsible for the covalent modification of CYP3A4.

Materials And Methods

Chemicals and Reagents. INF and erdafitinib were purchased from MedChem Express (Monmouth Junction, NJ). Dexamethasone, ketoconazole, prednisolone, rivaroxaban, verapamil hydrochloride, glutathione (GSH), catalase safranin O and Tergitol-type NP40 were acquired from Sigma-Aldrich (St. Louis, MO). Midazolam was procured from Tocris Bioscience (Bristol, UK). Testosterone and sodium dithionite were purchased from Tokyo Chemical Industries (Tokyo, Japan). Potassium ferricyanide was obtained from VWR International (Leuven, Belgium). Human recombinant P450 3A4 and 3A5 supersomes (rhCYP3A4 and rhCYP3A5) coexpressing cytochrome b_5, NADPH P450 reductase, and the NADPH regenerating system comprising NADP+ and glucose-6-phosphate (G6P) (NADPH A) and glucose-6-phosphate dehydrogenase (G6PDH) (NADPH B) were purchased from Corning Gentest (Woburn, MA). High-performance liquid chromatography–grade acetonitrile was procured from Tedia Company Inc. (Fairfield, OH). Ultrapure water (type I) was obtained using a Milli-Q water purification system (Millipore Corporation, Bedford, MA). All other commercially available chemicals were of analytical or high-performance liquid chromatography–grade.

Substrate Depletion of INF in CYP3A4 and CYP3A5. All incubations described in this work were performed in 96-well plates. Incubation mixtures consisting of 20 pmol/ml rhCYP3A4 or rhCYP3A5, 1 μM INF, G6PDH, and 100 mM potassium phosphate buffer (pH 7.4) were prepared in triplicate. After preincubating at 37°C for 5 minutes, the reaction was initiated via the addition of NADP+/G6P. The final primary incubation mixture (100 μl) contained <1% v/v organic solvent. Subsequently, at various time intervals (0, 5, 10, 15, 30, 45, 60, 80, 100, and 120 minutes), an 80-μl aliquot of each incubation mixture was withdrawn and quenched with equal volumes of ice-cold acetonitrile spiked with 100 nM erdafitinib (internal standard). The quenched samples were then centrifuged at 4000*g* at 4°C for 30 minutes, after which aliquots of the supernatant were withdrawn to quantify the amount of INF remaining using LC/MS/MS.

Time-, Concentration-, and NADPH-Dependent Inactivation of CYP3A4. Enzyme inactivation kinetic assays were performed as described in our previous works (Tang et al., 2021a,b). Briefly, primary incubation mixtures comprising 20–40 pmol/ml rhCYP3A4, INF (0, 1, 2.5, 5, 15, and 25 μM), G6PDH, and 100 mM potassium phosphate buffer (pH 7.4) were prepared in triplicate. After preincubating at 37°C for 5 minutes, the reaction was initiated via the addition of NADP+/G6P. The final primary incubation mixture (100 μl) contained <1% v/v organic solvent. Subsequently, at various preincubation intervals (0, 3, 8, 15, 22, and 30 minutes), a 5-μl aliquot of each primary incubation mixture was sampled and transferred to 95 μl of prewarmed secondary incubation mixture consisting of a CYP3A-specific probe substrate, an NADPH regenerating system (1 mM), and 100 mM potassium phosphate buffer (pH 7.4). This yielded a 20-fold dilution. Specifically, three structurally disparate substrates of CYP3A at concentrations more than ~4× their respective K_m were included in our assay (i.e., 200 μM testosterone, 25 μM midazolam, and 50 μM rivaroxaban) (Supplemental Fig. 1). The secondary incubation mixtures were incubated at 37°C for an additional 10 minutes (for assays involving testosterone or

midazolam) or 2 hours (for experiments involving rivaroxaban). After which, an 80-μl aliquot was immediately withdrawn and quenched with equal volumes of ice-cold acetonitrile spiked with either 1 μM prednisolone (internal standard for quantification of 6β-hydroxytestosterone and 1'-hydroxymidazolam) or 4 μM dexamethasone (internal standard for quantification of hydroxylated rivaroxaban). The quenched samples were centrifuged at 4000g at 4°C for 30 minutes to obtain the supernatant for LC/MS/MS analysis. Negative control experiments were performed by substituting NADP+/G6P with 100 mM potassium phosphate buffer (pH 7.4). Additionally, parallel experiments involving rhCYP3A5 in place of rhCYP3A4 were also conducted to investigate whether INF exhibits any potential time-dependent inhibition against CYP3A5. The concentrations of the three structurally disparate probe substrates used in these experiments were identical to those employed in the CYP3A4 experiments.

Calculation of MBI Kinetic Parameters (K_I and k_{inact}). To derive the inactivation kinetic parameters (K_I and k_{inact}), the mean of triplicate peak area ratios was used to calculate the natural logarithm of percentage residual P450 enzyme activity normalized to vehicle, which was then plotted against preincubation time for each INF concentration. The resulting data points were fitted to linear regression, and the observed first-order inactivation rate constant (k_{obs}) was derived from the slope of the linear decline in CYP3A activity for each INF concentration. Specifically, in CYP3A MBI assays involving midazolam as the probe substrate, points from preincubation timepoints 0 to 15 minutes were used in the derivation of the k_{obs}. Whereas in assays comprising testosterone or rivaroxaban as the probe substrate, points throughout 0 to 30 minutes were used as the decline in enzymatic activity was determined to be linear even after 30 minutes of preincubation, after which a plot of k_{obs} against INF concentrations [I] allowed the fitting of inactivation kinetic parameters (K_I and k_{inact}) to nonlinear least-square regression based on eq. 1 in GraphPad 8.0.2 (San Diego, CA)

$$k_{obs} = \frac{k_{inact} \times [I]}{K_I + [I]}, \quad (1)$$

where k_{inact} represents the maximal inactivation rate constant; K_I is the concentration of the inactivator at half-maximum inactivation rate constant; and [I] is the in vitro concentration of the inactivator (INF). Equation 1 assumes that there is negligible change of [I] during the incubation period and that the loss of enzyme activity is purely commensurate with inactivation by INF. The ratio of k_{inact} to K_I was determined by dividing the mean values of k_{inact} by K_I. Lastly, the time required for half of the enzyme molecules to be inactivated ($t_{1/2}$) was determined by eq. 2.

$$t_{1/2} = \frac{ln2}{k_{inact}}. \quad (2)$$

Partition Ratio. Rivaroxaban was used as the probe substrate in the secondary incubation mixture in all subsequent CYP3A4 MBI assays described in this work. Primary incubation mixtures consisting of 100 pmol/ml rhCYP3A4, INF (0, 1, 2.5, 5, 15, 25, and 50 μM), G6PDH, and 100 mM potassium phosphate buffer (pH 7.4) were prepared in triplicates. After prewarming the mixture at 37°C for 5 minutes, the reaction was initiated via the addition of NADP+/G6P and incubated for 45 minutes to allow inactivation to go into completion. The final primary incubation mixture (50 μl) contained <1% v/v organic solvent. Thereafter, aliquots of the primary incubation mixture were withdrawn and transferred to the secondary incubation mixture (similar to that prepared for the inactivation experiments) and incubated at 37°C for another 2 hours. Samples were then quenched and assayed for residual enzyme activity as described above. The partition ratio was estimated as detailed in our previous study (Tang et al., 2021a,b). Briefly, the percentage of residual CYP3A4 activity was plotted against the molar ratio of INF to CYP3A4 concentration. The turnover number (partition ratio + 1) was obtained by extrapolating the intercept of the linear regression line plotted at lower ratios with the straight line plotted at higher ratios to the abscissa. Finally, the partition ratio was back calculated by subtracting the turnover number by a value of 1.

Substrate Protection. To investigate whether enzyme inactivation could be amenable to substrate protection, an alternative CYP3A substrate testosterone, at a concentration of 100 and 200 μM (corresponding to 1:4 and 1:8 molar ratio of INF:testosterone) or a potent direct inhibitor of CYP3A ketoconazole, at a concentration of 0.1 and 1 μM (approximately 1× and 10× its K_i value), was introduced separately in triplicate to the primary incubation mixture containing 40 pmol/ml rhCYP3A4, 25 μM INF, G6PDH, and 100 mM potassium phosphate buffer (pH 7.4). The enzymatic reaction was initiated by the addition of NADP+/G6P after preincubation at 37°C for 5 minutes. Aliquots were withdrawn at different preincubation time points (0, 3, 8, and 15 minutes), transferred to the secondary incubation mixture, and the mixtures were subsequently assayed for residual CYP3A4 enzymatic activity as described above. Primary incubation mixtures that excluded the addition of either testosterone, ketoconazole, or both INF and testosterone or ketoconazole served as the negative controls.

Effect of Exogenous Nucleophile and Scavenger of ROS on Inactivation. The exogenous nucleophilic trapping agent GSH (2 mM) was added to the primary incubation mixture containing 40 pmol/ml rhCYP3A4, 25 μM INF, G6PDH, and 100 mM potassium phosphate buffer (pH 7.4). After preincubating at 37°C for 5 minutes, the enzymatic reaction was initiated via the addition of NADP+/G6P. At specific preincubation time points (0, 3, 8, and 15 minutes), aliquots were transferred to the secondary incubation mixtures and subsequently assayed for residual CYP3A4 enzymatic activity as previously described. Negative controls were prepared without both INF and GSH or only without GSH in the primary incubation mixture. Parallel experiments involving the incorporation of catalase (800 U/ml) in place of GSH were also performed to investigate the effects of scavenger of ROS on the inactivation of CYP3A4.

Reversibility of Inactivation. The reversibility of CYP3A4 inactivation was interrogated by two distinct approaches; namely equilibrium dialysis and oxidation by potassium ferricyanide, as described in detail in our previous works (Hong et al., 2016; Karkhanis et al., 2016; Tang et al., 2021b). In the dialysis experiments, triplicate primary incubation mixtures comprising 40 pmol/ml rhCYP3A4, 25 μM INF, G6PDH, and 100 mM potassium phosphate buffer (pH 7.4) were prewarmed at 37°C for 5 minutes. Enzymatic reaction was initiated by the addition of NADP+/G6P and allowed to proceed for 30 minutes, after which a 5-μl aliquot was transferred to 95 μl of the secondary incubation mixture yielding a 20-fold dilution. Concurrently, 90 μl of the remaining primary incubation mixture was transferred to a Slide-A-Lyzer mini dialysis device (0.1 ml, molecular weight cutoff of 10,000; Pierce Chemical Co., Rockford, IL) and placed in a glass beaker filled with 500 ml of ice-cold 100 mM potassium phosphate buffer (pH 7.4). The buffer system was maintained on ice (4°C) with constant gentle stirring and accompanied by one fresh buffer change at the second hour. After 4 hours, 5 μl of the dialyzed mixture was transferred to each prewarmed secondary incubation well. All secondary mixtures were further incubated at 37°C for 2 hours and subsequently assayed for residual CYP3A4 enzymatic activity as previously described.

Conversely, in the experiments involving potassium ferricyanide, a series of three sequential incubations were conducted. Briefly, the primary incubation comprised 40 pmol/ml rhCYP3A4, G6PDH, and 100 mM potassium phosphate buffer (pH 7.4) in the presence or absence of 25 μM INF. After initiation of the reaction with the addition of NADP+/G6P and incubation at 37°C for either 0 or 30 minutes, 20 μl of the primary incubation mixture was aliquoted into an equal volume of secondary incubation mixture containing 100 mM potassium phosphate buffer (pH 7.4) with or without 2 mM potassium ferricyanide. The secondary mixtures were then allowed to incubate at 37°C for another 10 minutes. Thereafter, 10 μl of the mixture was withdrawn and diluted 10-fold into a tertiary incubation mixture containing 50 μM rivaroxaban (probe substrate), an NADPH regenerating system (1 mM), and 100 mM potassium phosphate buffer (pH 7.4). The reaction mixture was further incubated at 37°C for another 2 hours and subsequently assayed for residual CYP3A4 activity as previously described. The percentage of CYP3A4 metabolic activity remaining after 0 or 30 minutes incubation with INF compared with the corresponding controls in the absence of INF was calculated using eqs. 3 and 4 respectively.

$$\%\ \text{control}_{0\ min} = \frac{v_{(0\text{min},(+)INF)}}{v_{(0\text{min},(-)INF)}} \times 100 \quad (3)$$

$$\%\ \text{control}_{30\ min} = \frac{v_{(30\text{min},(+)INF)}}{v_{(30\text{min},(-)INF)}} \times 100, \quad (4)$$

where v represents the residual CYP3A4 activity. Thereafter, % restoration of metabolic activity of CYP3A4 was derived by subtracting % $\text{control}_{30\ min}$ in the presence of potassium ferricyanide with the corresponding values obtained in the absence of potassium ferricyanide.

Spectral Difference Scanning. Incubation mixtures (200 μl) containing 200 pmol/ml rhCYP3A4, 25 μM INF, G6PDH, and 100 mM potassium phosphate buffer (pH 7.4) were prepared and preincubated at 37°C for 5 minutes. Thereafter, the enzymatic reaction was initiated via the addition of NADP+/G6P and immediately scanned from 400 to 500 nm at 5-minute intervals over a 1-hour duration using a Hidex Sense microplate reader (Hidex, Turku, Finland) maintained at a constant 37°C. The spectral differences were obtained by comparing the UV absorbances between the sample and reference wells, which consisted of vehicle in place of INF. Positive control wells were also prepared using 10 μM verapamil, a known quasi-irreversible of CYP3A4. Finally, the degree of metabolite-intermediate (MI) complex formation was also quantitatively assessed by measuring the absorbance difference between 454 and 490 nm with time.

Reduced CO-Difference Spectroscopy. Reduced CO-difference spectroscopy was performed as previously described (Chan et al., 2012) with slight modifications. Briefly, incubation mixtures (50 μl) comprising 200 pmol/ml rhCYP3A4, 25 μM INF, G6PDH, and 100 mM potassium phosphate buffer (pH 7.4) were prepared and prewarmed at 37°C for 5 minutes. The enzymatic reaction was then initiated via the addition of NADP+/G6P and allowed to proceed for 30 minutes, after which the reaction was terminated via the addition of 450 ml ice-cold quenching buffer consisting of 1 mM EDTA, 20% glycerol, 1% Tergitol-type NP40, 2 mM safranin O, and 100 mM potassium phosphate buffer (pH 7.4). The quenched mixture was evenly split into two 250-μl tubes (sample and reference tubes), and CO gas was gently bubbled into the sample tube and stopped after about 60 bubbles had been introduced into the mixture. Thereafter, approximately 1 mg of sodium dithionite was added to both tubes, and 200 μl of the mixture was transferred out from each tube after gentle inversion into a 96-well plate. The reduced CO-difference spectra for the sample and reference wells were recorded by scanning from 400 to 500 nm using a Hidex Sense microplate reader (Hidex, Turku, Finland). Negative controls were prepared by excluding NADPH from the incubation mixture.

GSH Trapping. GSH trapping experiments were performed as previously outlined (Teng et al., 2010; Hong et al., 2016). Incubation mixtures (500 μl) containing 50 pmol/ml rhCYP3A4, 25 μM INF, G6PDH, 50 mM GSH, and 100 mM potassium phosphate buffer (pH 7.4) were prepared and preincubated at 37°C for 5 minutes. The reaction was then initiated via the addition of NADP+/G6P and incubated at 37°C for 1 hour. Thereafter, 500 μl of ice-cold acetonitrile was added to quench the reaction. The resulting mixture was centrifuged at 14,000*g* at 4°C for 15 minutes, after which the supernatant was transferred to a new microcentrifuge tube and dried under a gentle stream of nitrogen gas (TurboVap LV; Caliper Life Science, Hopkinton, MA). The residue was subsequently reconstituted with 60 μl of ACN-water mixture (3:7), vortexed, and centrifuged at 14,000*g* at 4°C for 15 minutes. The supernatant was then carefully removed for LC/MS/MS analysis. Samples which omitted the inclusion of INF in the incubation mixture served as the negative controls.

Covalent Docking of INF to CYP3A4 and CYP3A5. Covalent docking of INF to CYP3A4 and CYP3A5 was performed as described in our previous works (Tang et al., 2021b,c). Briefly, three-dimensional coordinates of INF were obtained from the PubChem database (Kim et al., 2019), from which the *p*-benzoquinonediimine intermediate was derived using LigPrep (Schrödinger, New York) and covalently docked to CYP3A4 and CYP3A5 using CovDock (Zhu et al., 2014) in the Schrödinger suite. The protein dataset for CYP3A4 was composed of the previously curated 49 high-resolution crystal structures (<3 Å) (Tang et al., 2021b), whereas the protein dataset for CYP3A5 consisted of the two reported crystal structures and an ensemble of 28 molecular dynamics simulation frames generated from our previous trajectory clustering analyses (Tang et al., 2021c).

Reversible Inhibition of CYP3A4 by INF. The reversible inhibition of INF against CYP3A4 was also investigated using the same three structurally distinct CYP3A probe substrates as described in the MBI assays above. Reaction mixtures for IC_{50} experiments consisted of either 10–20 pmol/ml rhCYP3A4, INF (0.01–50 μM), probe substrate (50 μM testosterone, 3 μM midazolam, or 10 μM rivaroxaban, representing concentrations at their respective K_m values), G6PDH, and 100 mM potassium phosphate buffer (pH 7.4). Whereas reaction mixtures for K_i experiments comprised 20 pmol/ml rCYP3A4, INF (0, 0.03, 0.06, 1, and 3 μM), rivaroxaban (2.5, 5, 15, and 30 μM), G6PDH, and 100 mM potassium phosphate buffer (pH 7.4). After prewarming at 37°C for 5 minutes, the reaction was initiated via the addition of NADP+/G6P, yielding a final primary incubation mixture (100 μl) with <1% v/v organic solvent. The reaction mixture was incubated at 37°C for 10 minutes (for assays involving testosterone or midazolam) or 2 hours (for experiments involving rivaroxaban), after which aliquots of the samples were quenched, centrifuged, and subjected to LC/MS/MS

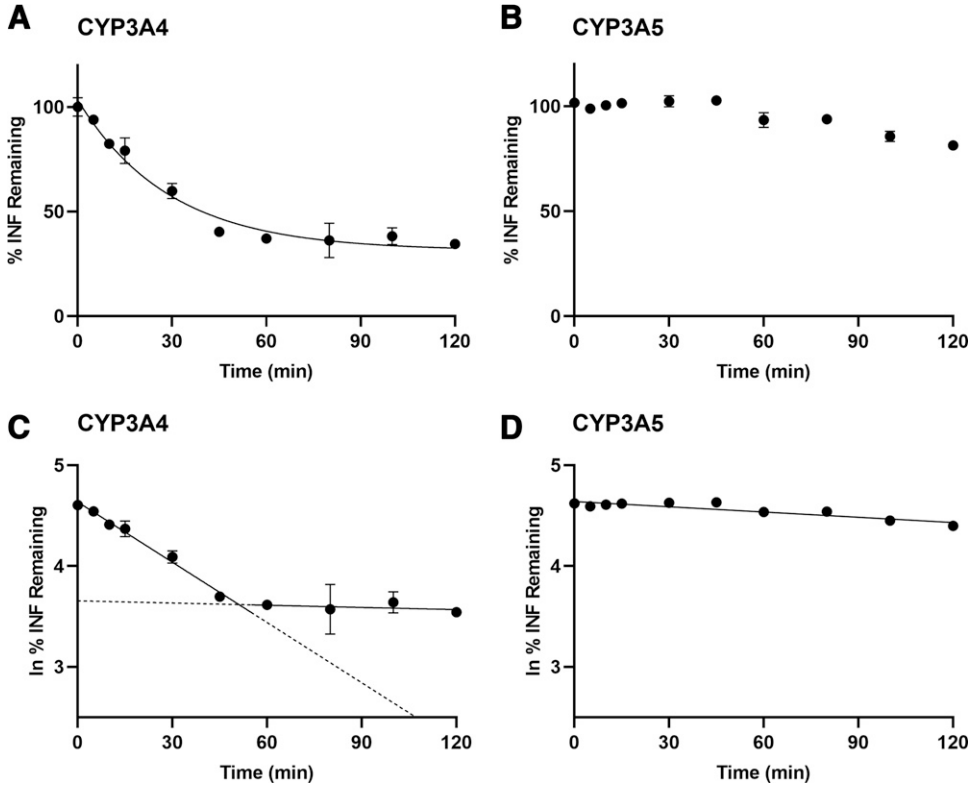

Fig. 2. Substrate depletion of INF by CYP3A. Percentage of INF remaining against time in the presence of (A) CYP3A4 and (B) CYP3A5 plotted on a linear scale and the corresponding substrate depletion graphs of INF in the presence of (C) CYP3A4 and (D) CYP3A5 as plotted on a seminatural logarithmic scale. Each point in (A–D) represents the mean and S.D. of triplicate experiments.

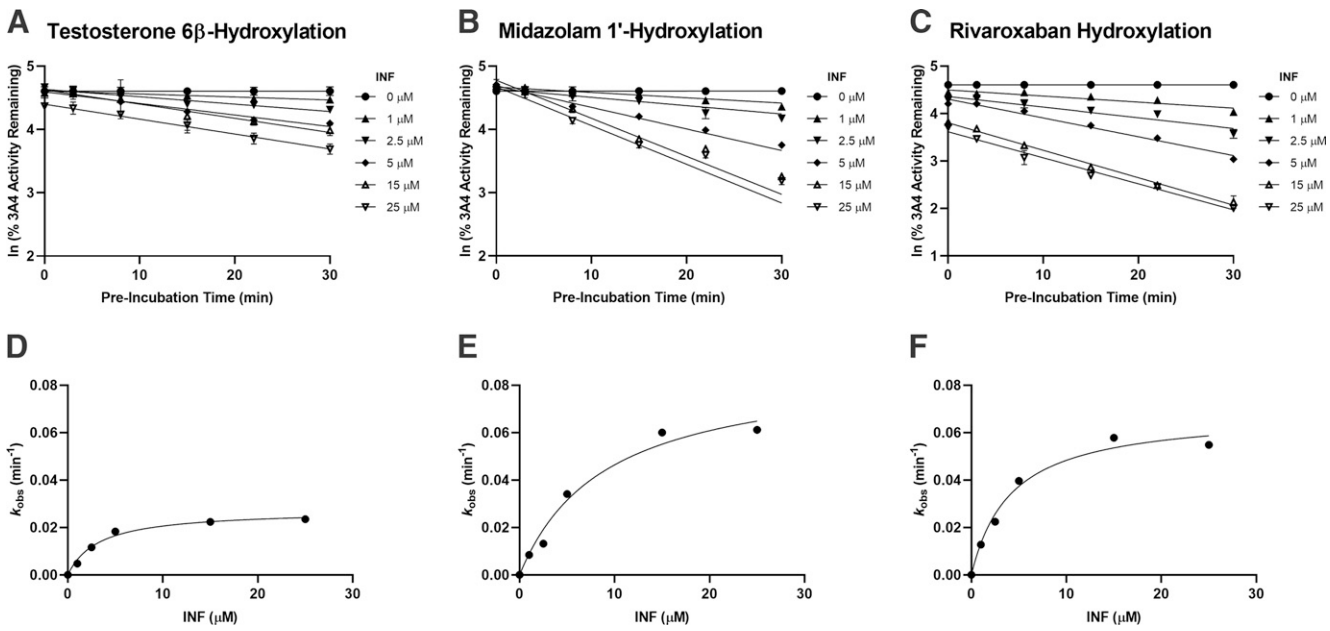

Fig. 3. Time- and concentration-dependent inactivation of CYP3A4 by INF using (A) testosterone, (B) midazolam, and (C) rivaroxaban as probe substrates. Nonlinear regression of k_{obs} versus INF concentration yielded K_I and k_{inact} values of 3.26 ± 0.61 μM and 0.027 ± 0.002 minute^{-1} when (D) testosterone was used as the probe substrate, 9.03 ± 2.85 μM and 0.088 ± 0.011 minute^{-1} when (E) midazolam was harnessed as the probe substrate, and 4.17 ± 0.93 μM and 0.068 ± 0.005 minute^{-1} when (F) rivaroxaban was employed as probe substrates respectively. Each point in (A–C) represents the mean and S.D. of triplicate experiments.

analysis for the quantitation of either 6β-hydroxytestosterone, 1'-hydroxymidazolam, or hydroxylated rivaroxaban.

Calculation of Reversible Inhibition Kinetic Parameters (IC_{50} and K_i) and Determination of Modes of Inhibition. The IC_{50} was determined using the log(inhibitor) versus response–variable slope (four parameters) model based on eq. 5 in GraphPad 8.0.2 (San Diego, CA)

$$Y = min + \frac{(max - min)}{(1+10^{(logIC_{50}-[I])\ \times\ Hill\ Slope})}, \quad (5)$$

where IC_{50} represents the half-maximal inhibitory concentration, min is the minimum effect, max is the maximum effect, [I] is the in vitro concentration of the reversible inhibitor, Hill slope is the Hill coefficient, and Y is the % enzyme activity compared to control.

Apparent K_i values were derived by nonlinear least-square regression analysis of hydroxylated rivaroxaban formation data (expressed in peak area ratio) collected at various rivaroxaban and INF concentration using eq. 6 for noncompetitive inhibition in GraphPad 8.0.2 (San Diego, CA). The mode of reversible inhibition was determined based on statistical evaluation of the Michaelis-Menten plots by corrected Akaike's information criterion and further verified via visual inspection of the transformed Lineweaver-Burk plots,

$$v = \frac{V_{max}}{\left(1 + \frac{[I]}{K_i}\right) \times \left(1 + \frac{K_m}{[S]}\right)}, \quad (6)$$

where v is the rate of enzyme activity, V_{max} (maximum rate of reaction) and K_m (Michaelis constant) are kinetic constants for substrate metabolism; [S] is the in vitro concentration of substrate (rivaroxaban); [I] is the in vitro concentration of inhibitor (INF), and K_i is the equilibrium dissociation constant for the enzyme-inhibitor complex.

Measurement of INF and Residual P450 Activity by LC/MS/MS. All samples were analyzed using the liquid chromatography tandem mass spectrometry (LC/MS/MS) system consisting of an Agilent 1290 Infinity ultra-high pressure liquid chromatography (Agilent Technologies Inc., Santa Clara, CA) interfaced with an AB SCIEX QTRAP 3500 tandem mass spectrometry (MS/MS) (AB SCIEX, Framingham, MA). Chromatographic separation of INF and erdafitinib (internal standard) in the substrate depletion assay was achieved with an ACQUITY ultra-performance liquid chromatography ethylene bridged hybrid

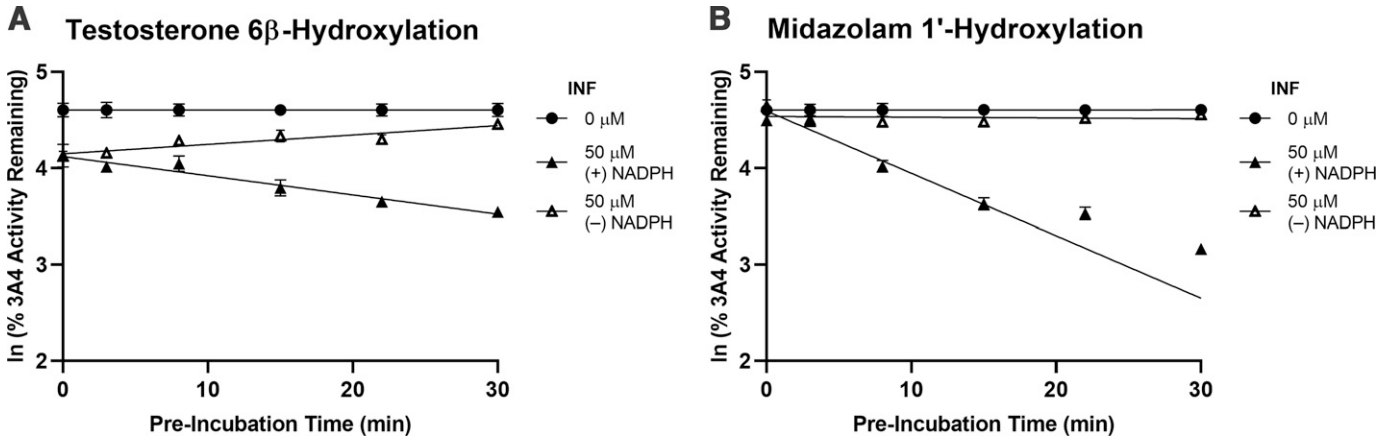

Fig. 4. Cofactor NADPH-dependent inactivation of CYP3A4 by INF using (A) testosterone and (B) midazolam as probe substrates. Each point in (A and B) represents the mean and S.D. of triplicate experiments.

TABLE 1

CYP3A4 inactivation kinetic parameters for INF derived using either testosterone 6β-hydroxylation, midazolam 1'-hydroxylation, or morpholinone hydroxylation of rivaroxaban as surrogate markers of residual CYP3A activity
Data are presented as means ± S.D.

Probe Substrate	K_I	k_{inact}	k_{inact}/K_I	$t_{1/2}$	Partition Ratio
	μM	min^{-1}	$min^{-1}mM^{-1}$	min	
Testosterone	3.26 ± 0.61	0.027 ± 0.002	8.4	25.40	N.D
Midazolam	9.03 ± 2.85	0.088 ± 0.011	9.8	7.85	N.D
Rivaroxaban	4.17 ± 0.93	0.068 ± 0.005	16.4	10.12	41

N.D., not determined.

(BEH) C_{18}, 1.7 μM, 2.2 × 100 mm column (Waters, Milford, MA), whereas a similar but shorter 50-mm column was used for the chromatographic separation of the rest of the analytes and internal standards described in this work. The aqueous mobile phase (A) was 0.1% formic acid in water, whereas the organic mobile phase (B) was 0.1% formic acid in acetonitrile. Mobile phases were delivered at a flow rate of 0.5 ml/min. The column and sample temperature were set at 45°C and 4°C, respectively. The gradient elution conditions were as follows: linear gradient from 20% to 80% B (0–1.20 minutes), isocratic at 100% B (1.21–2.00 minutes), and isocratic at 20% B (2.01–2.50 minutes). All analytes were detected in positive electrospray ionization (ESI) mode. The source-dependent MS parameters were as follows: ion spray voltage = 5500 V; source temperature = 500°C; curtain gas (CUR) = 25 psi; ion source gas 1 (sheath gas) = 30 psi; ion source gas 2 (drying gas) = 30 psi. The multiple reaction monitoring transitions and compound-dependent MS parameters of the analytes are summarized in Supplemental Table 1. Chromatographic peak integration was performed using Analyst software version 1.6.2 (Applied Biosystems). For all LC/MS/MS analyses, the peak area of the analyte was expressed as a ratio to the peak area of the internal standard.

Detection of GSH Adducts. GSH adduct of putative reactive electrophilic intermediate of INF was analyzed using the LC/MS/MS system consisting of an Agilent 1290 Infinity ultra-high pressure liquid chromatography (Agilent Technologies Inc., Santa Clara, CA) interfaced with an AB SCIEX QTRAP 5500 MS/MS (AB SCIEX, Framingham, MA). Chromatographic separation was achieved on an ACQUITY ultra-performance liquid chromatography BEH C_{18}, 1.7 μM, 2.2 × 100 mm column (Waters, Milford, MA). The aqueous mobile phase (A) was 0.1% formic acid in water, whereas the organic mobile phase (B) was 0.1% formic acid in acetonitrile. Mobile phases were delivered at a flow rate of 0.45 ml/min. The column and sample temperature were set at 45°C and 4°C, respectively. The gradient elution conditions were as follows: linear gradient 5% to 60% B (0–6.25 minutes), isocratic at 95% B (6.26–7.00 minutes) and isocratic at 5% B (7.01–8.00 minutes). An information-dependent acquisition experiment was conducted to detect INF-derived GSH conjugates including precursor ion scan (PIS) of *m/z* 272 in negative ESI mode and neutral loss scan (NL) of 129 Da in positive ESI mode. Enhanced product ion (EPI) scan was subsequently performed for all potential GSH adducts identified. The source-dependent MS parameters used were as follows: ion spray voltage = 5000 V; source temperature =

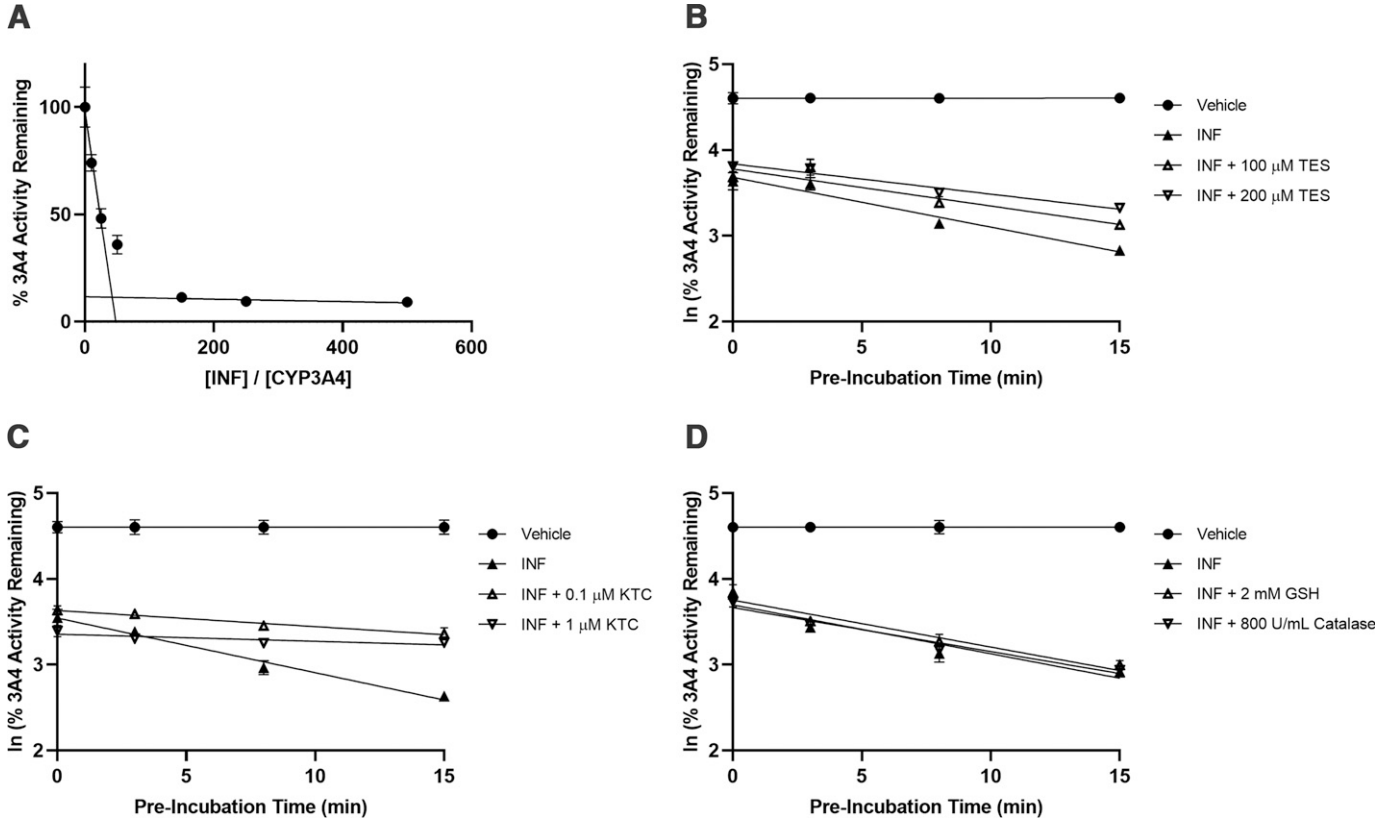

Fig. 5. (A) Partition ratio for the inactivation of CYP3A4 by INF estimated to be 41 was determined by extrapolating the intercept of the linear regression line at lower ratios and the straight line for the high ratios to the x-axis. Inactivation of CYP3A4 was attenuated in the presence of (B) an alternative CYP3A substrate testosterone (TES) and (C) a direct CYP3A inhibitor ketoconazole (KTC). (D) Conversely, the presence of either GSH or catalase did not protect against enzymatic inactivation. Each point in (A–D) represents the mean and S.D. of triplicate experiments.

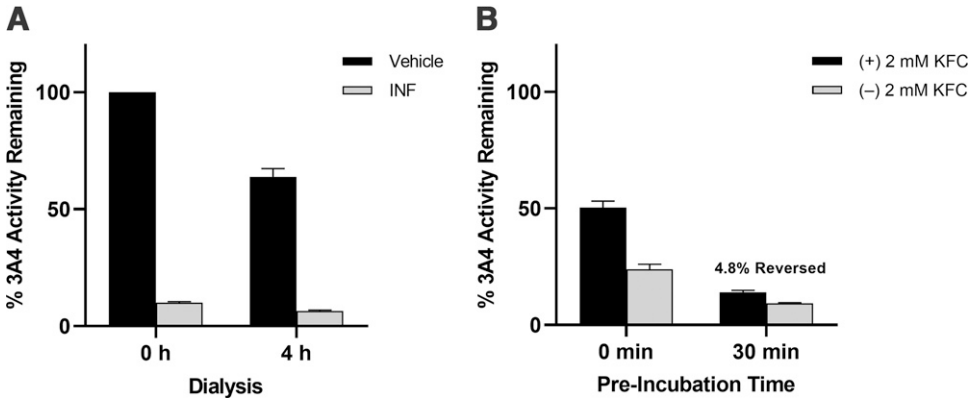

Fig. 6. (A) Percentage activity of CYP3A4 remaining did not increase after extensive dialysis at 4°C for 4 hours. (B) Potassium ferricyanide (KFC) only restored the metabolic activity of CYP3A4 by a modest 4.8 ± 1.11% after a 30-minute incubation with 25 μM INF. Results from both graphs show the mean and S.D. of two independent experiments conducted in triplicates.

650°C; CUR = 20 psi; ion source gas 1 (sheath gas) = 45 psi; ion source gas 2 (drying gas) = 60 psi.

Accurate mass measurement of the prospective INF-derived GSH adduct identified in the GSH trapping experiments was performed using an ACQUITY ultra-performance liquid chromatography system (Waters, Milford, MA) coupled to a quadrupole time-of-flight (QTOF) high-resolution MS (AB SCIEX Triple-TOF 5600 MS; AB SCIEX, Framingham, MA) equipped with a DuoSpray ion source (AB SCIEX, Framingham, MA). Chromatographic separation was achieved on an ACQUITY ultra-performance liquid chromatography BEH C_{18}, 1.7 μM, 2.2 × 100 mm column (Waters, Milford, MA). The mobile phases, flow rate, temperature, and gradient elution conditions were identical to those employed in the LC/MS/MS experiments described earlier in this section. External mass calibration was performed at the start and after every five samples with the APCI Positive Calibration Solution (AB SCIEX, Framingham, MA) to ensure high mass accuracy and reproducibility. Other source-dependent MS parameters are as follows; ion spray voltage floating = 5500 V; source temperature = 500°C; CUR = 30 psi; ion source gas 1 (sheath gas) = 55 psi; ion source gas 2 (drying gas) = 60 psi, whereas the collision energy was set to 38 V with a collision energy spread of 5 V. The QTOF-MS data were extracted and analyzed using the PeakView software version 2.2 (AB SCIEX, Framingham, MA).

Results

INF Substrate Depletion by CYP3A4 and CYP3A5. To elucidate any potential time-dependent inhibition of CYP3A by INF, we first monitored the depletion of INF over time by CYP3A4 and CYP3A5. Our results demonstrated that both CYP3A isoforms were capable of metabolizing INF, but with vastly different efficiencies. Specifically, the percentages of INF remaining after 2 hours were 34.54 ± 1.33% in CYP3A4 incubations (Fig. 2A) and 81.34 ± 1.80% in CYP3A5 incubations (Fig. 2B). Interestingly, two distinct phases were observed in the log-transformed substrate depletion profile of INF for CYP3A4, but not with CYP3A5 (Fig. 2, C and D). A comparison of the elimination rate constants in the initial portion of incubation revealed that INF was metabolized ∼12 times faster by CYP3A4 as compared with CYP3A5 (i.e., k_{CYP3A4} = 0.0200 ± 0.0009 minute^{-1} compared with k_{CYP3A5} = 0.0017 ± 0.0002 minute^{-1}). However, after approximately 45 minutes of incubation, there was a drastic reduction in the rate of metabolism by CYP3A4 which point toward possible time-dependent inhibition.

Time-, Concentration-, and NADPH-Dependent Inactivation of CYP3A4. As our earlier substrate depletion experiments hinted that INF could evoke time-dependent inhibition of CYP3A4, we proceeded with a deeper characterization of its inactivation kinetics using the FDA-recommended CYP3A substrates testosterone and midazolam. In addition to these prototypical substrates, we also adopted rivaroxaban as a clinically relevant probe substrate of CYP3A. Our findings revealed that INF inactivated CYP3A4 in a time- and concentration-dependent manner for all three probe substrates of CYP3A used (Fig. 3, A–C), with the most profound loss of enzyme activity obtained when 25 μM INF was preincubated with CYP3A4 for 30 minutes. Moreover, the omission of NADPH, which functions as a cofactor in P450-mediated metabolic reactions, abrogated the loss of CYP3A-mediated testosterone 6β-hydroxylase and 1'-midazolam hydroxylase activity when preincubated with 50 μM INF for up to 30 minutes (Fig. 4). This apparent dependence on NADPH implied that prior metabolic activation of INF was a key molecular-initiating event leading to the eventual inactivation of CYP3A4. Furthermore, as the k_{obs} determined from the gradients of each of the included concentrations of INF approached a maximum

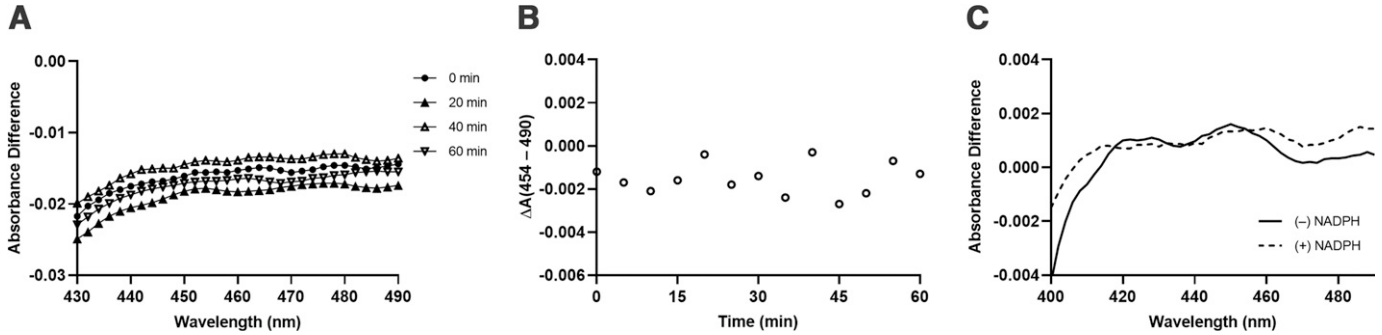

Fig. 7. (A) Spectral difference measured over 60 minutes failed to elicit a Soret peak in the absorbance ranges of 448–458 nm for CYP3A4 incubated with 25 μM INF. (B) Similarly, a comparison of the absorbance at the reference of 454 nm against the isosbestic point at 490 nm failed to demonstrate an increase in the extent of MI complex formation over time. (C) Reduced CO-difference spectrum of CYP3A4 after incubation with 25 μM INF for 30 minutes in the absence and presence of cofactor NADPH.

TABLE 2

Accurate mass measurement of the parent and product ions of INF-derived GSH adduct (*m/z* 865) using a mass tolerance of 5 ppm

Proposed Elemental Composition	Theoretical *m/z*	Experimental *m/z*	Mass Accuracy	
			Δ*Da*	Δ*ppm*
$C_{36}H_{46}N_{10}O_9SCl_2$	865.2620	865.2599	−0.0021	−2.4
$C_{36}H_{44}N_{10}O_8SCl_2$	847.2514	847.2487	−0.0027	−3.2
$C_{31}H_{39}N_9O_6SCl_2$	736.2194	736.2176	−0.0018	−2.4
$C_{27}H_{39}N_9O_6S$	618.2817	618.2804	−0.0013	−2.1
$C_{27}H_{37}N_9O_5S$	600.2711	600.2689	−0.0022	−3.7
$C_{22}H_{32}N_8O_3S$	489.2391	489.2378	−0.0013	−2.6
$C_{17}H_{24}N_6S$	345.1856	345.1848	−0.0008	−2.3

inactivation rate constant (k_{inact}) (Fig. 3, D–F), it denoted that the loss of CYP3A4 activity elicited by INF followed pseudo-first order kinetics. At this outset, the inactivation kinetic parameters (K_I and k_{inact}) of INF derived from the Kitz-Wilson plot (Kitz and Wilson, 1962) were 3.26 ± 0.61 μM and 0.027 ± 0.002 minute^{-1}, respectively, when testosterone was used as the probe substrate, 9.03 ± 2.85 μM and 0.088 ± 0.011, respectively, when midazolam was harnessed as the probe substrate, and 4.17 ± 0.93 μM and 0.068 ± 0.005 minute^{-1} when rivaroxaban was employed as the probe substrate. This in turn yielded corresponding k_{inact}/K_I ratios of 8.4, 9.8, and 16.4 minute^{-1}mM^{-1} and inactivation $t_{1/2}$ of 25.40, 7.85, and 10.12 minutes, respectively. All reported values of K_I, k_{inact}, k_{inact}/K_I ratio, and $t_{1/2}$ are summarized in Table 1. Conversely, there was a lack of time- or concentration-dependent reduction of CYP3A5 activity by INF in all three probe substrates used (Supplemental Fig. 2, A–C).

Partition Ratio. A titration method previously described (Silverman, 1995) was adopted, which determined the turnover number for the inactivation of CYP3A4 to be ∼42 (Fig. 5A). This, in turn, corresponded to a partition ratio of 41 (Table 1).

Substrate Protection. Inactivation of CYP3A4 by INF was protected in the presence of both an alternative substrate and direct inhibitor of CYP3A. Coincubation with either testosterone (Fig. 5B) or ketoconazole (Fig. 5C) attenuated the rate of inactivation by INF as illustrated by the diminished rate of enzyme inactivation with time. Furthermore, the magnitude of substrate protection conferred appeared to be dose-dependent, wherein inactivation was completely abolished when 1 μM ketoconazole was coincubated with INF and CYP3A4 in the primary incubation mixture.

Effect of Exogenous Nucleophile and Scavenger of ROS on Inactivation. The incorporation of GSH or catalase had no appreciable effect on the rate of enzyme inactivation elicited by INF. As evident in Fig. 5D, CYP3A4 was inactivated to a similar extent in incubation mixtures comprising INF alone.

Reversibility of Inactivation. To establish whether the inactivation of CYP3A4 by INF is quasi-irreversible or irreversible, the specific nature of inactivation was interrogated via equilibrium dialysis and oxidation with potassium ferricyanide. In the former, the magnitude of CYP3A4 activity was not restored after dialysis at 4°C for 4 hours

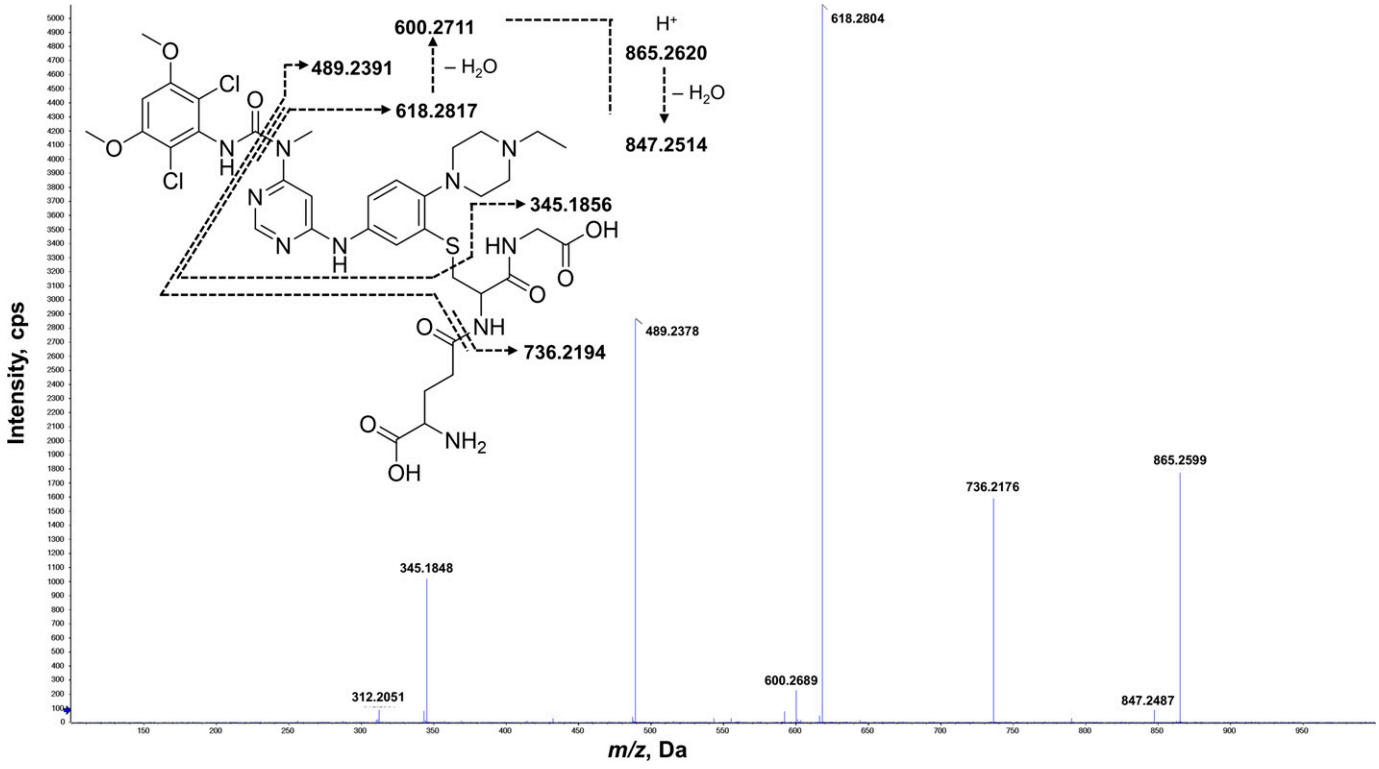

Fig. 8. Proposed accurate mass fragmentation pattern of the INF-derived GSH adduct. The MS/MS spectrum depicts the experimental *m/z* values, whereas the chemical structure illustrates the theoretical accurate *m/z* values of the parent and product ions of the adduct as outlined in Table 2 using a mass tolerance of 5 ppm.

TABLE 3
Summary of covalent docking scores for INF

P450 Isoform	Residue	PDB/Cluster ID	Docking Score	Minimum Distance between INF and F-F' Loop (□□□)
CYP3A4	Cys239	4I4H[b]	-4.7[a]	3.1
		4I3Q[b]	-4.6	3.3
		4K9W[b]	-4.4	3.0
		5A1P[b]	-4.1	3.3
		3NXU[b]	-4.1	3.3
		1TQN[b]	-3.4	3.1
CYP3A5	Ser239	Cluster-13[b]	-5.4[a]	3.1
		Cluster-18[c]	-3.6	3.2

[a]PDB/Cluster ID with best covalent docking score for a given residue position.
[b]F-F' loop in closed conformation (see *Discussion*).
[c]F-F' loop in open conformation (see *Discussion*).

(Fig. 6A). Rather, the marginal decrease in residual enzyme activity observed postdialysis could be ascribed to enzymatic degradation that might have occurred during dialysis as confirmed in vehicle control experiments. With regards to the latter, oxidation with potassium ferricyanide after a 30-minute preincubation with 25 μM INF restored the metabolic activity of CYP3A4 by a modest 4.8% ± 1.11% (Fig. 6B).

Spectral Difference Scanning. There was a lack of an observable peak in the Soret region (448–458 nm) associated with the formation of quasi-irreversible MI complexes when incubation mixtures containing INF and CYP3A4 were scanned from 400 to 500 nm at 5-minute intervals for 1 hour (Fig. 7A) (Polasek and Miners, 2008). Moreover, tracking the increase in absorbance between 454 nm and the isosbestic point at 490 nm further substantiated the lack of MI complex formation with INF (Fig. 7B). In contrast, control experiments involving verapamil (a known quasi-irreversible inactivator of CYP3A4) produced an observable Soret peak and a time-dependent increase in absorbance in the spectral differences between 454 and 490 nm that correlates with the extent of MI complex formation (Supplemental Fig. 3, A and B).

Reduced CO-Difference Spectroscopy. To determine whether the underlying mechanism of inactivation results from destruction of the prosthetic heme, reduced CO-difference spectroscopy was conducted to investigate the ability of CYP3A4 to bind CO. It is well established that the interaction between CO and ferrous (reduced) form of P450 produces a complex with a spectrally detectable peak at 450 nm (Omura and Sato, 1964). Consequently, any reduction of this peak arising from incubation with INF in a catalytically competent system hints at possible heme modification. Here, our findings demonstrate that, although there was a decrease in the reduced CO binding spectrum after incubation of CYP3A4 with INF in the presence of NADPH, it was somewhat marginal (Fig. 7C). Taken together, it implied that, although a small fraction of the reactive intermediate may irrevocably modify the prosthetic heme (i.e., via covalent alkylation and/or bleaching), it likely did not represent the major mode of inactivation. Rather, the predominant mechanism of inactivation by INF may be due to covalent adduction of the CYP3A4 apoprotein.

GSH Trapping. A GSH trapping assay was subsequently performed by fortifying the reaction mixtures with the nucleophilic trapping agent GSH to search for electrophilic reactive intermediates of INF that may be potentially implicated in the irreversible covalent adduction of the CYP3A4 apoprotein. Two survey scans, namely PIS at *m/z* 272 in negative mode and NL of 129 Da in positive mode (Baillie and Davis, 1993; Dieckhaus et al., 2005), were employed. These two well established survey scans, which monitor the loss of the deprotonated γ-glutamyl-dehydroalanyl-glycine and pyroglutamic acid moiety from GSH respectively, are frequently used by pharmaceutical scientists during drug discovery to identify drug candidates that pose potential metabolic liabilities. One peak suggestive of an INF-derived GSH adduct (retention time: 3.77 minutes) with an MH^+ ion at *m/z* of 865 and a characteristic dual chlorine isotopic pattern was detected in both the PIS at *m/z* 272 in ESI negative mode (Supplemental Fig. 4) and NL of 129 Da in positive ESI mode (Supplemental Fig. 5) but was absent in negative control samples lacking INF. The resultant EPI scan generated from this prospective INF-derived GSH adduct yielded a spectrum that was characteristic of collision-induced dissociation fragmentation of a GSH adduct due to the neutral mass loss of 129 Da corresponding to the loss of a pyroglutamate moiety in GSH (Supplemental Figs. 4 and 5). To further confirm the identity of the potential GSH adduct, accurate mass measurements were performed. As expected, we were able to recapitulate the nominal mass patterns generated using the QTRAP-MS when the GSH adduct was subjected to accurate mass measurements using the QTOF-MS. The proposed elemental composition, theoretical and experimental exact *m/z*, and mass accuracy (in both ΔDa and Δppm) of the GSH adduct are summarized in Table 2. Additionally, the accurate mass MS/MS spectrum and proposed fragmentation pattern of the INF-derived GSH adduct are shown in Fig. 8.

Covalent Docking of INF to CYP3A4 and CYP3A5. Covalent docking was performed to glean mechanistic insights on the plausible structural determinants underscoring the diverging MBI susceptibilities of CYP3A4 and CYP3A5 by INF. Our bioinformatics analyses previously identified Cys239 in CYP3A4 as an accessible

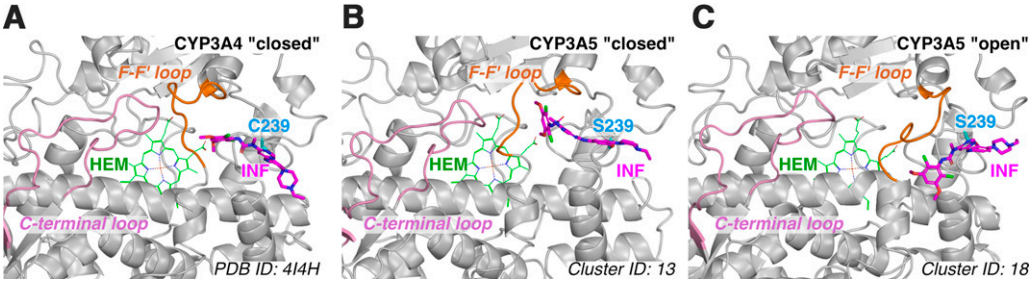

Fig. 9. Covalent adduction of INF to CYP3A4 and CYP3A5. Molecular plots illustrating the top scored binding poses for INF adducts at (A) Cys239 in the "closed" conformation of CYP3A4 (Protein Data Bank ID: 414H) and (B and C) Ser239 in both the "closed" and "open" conformations of CYP3A5 (cluster-13 and cluster-18, respectively). In all three instances, the 2,6-dichloro-3,5-dimethoxy-phenyl moiety of INF is visibly oriented toward the F-F' loop.

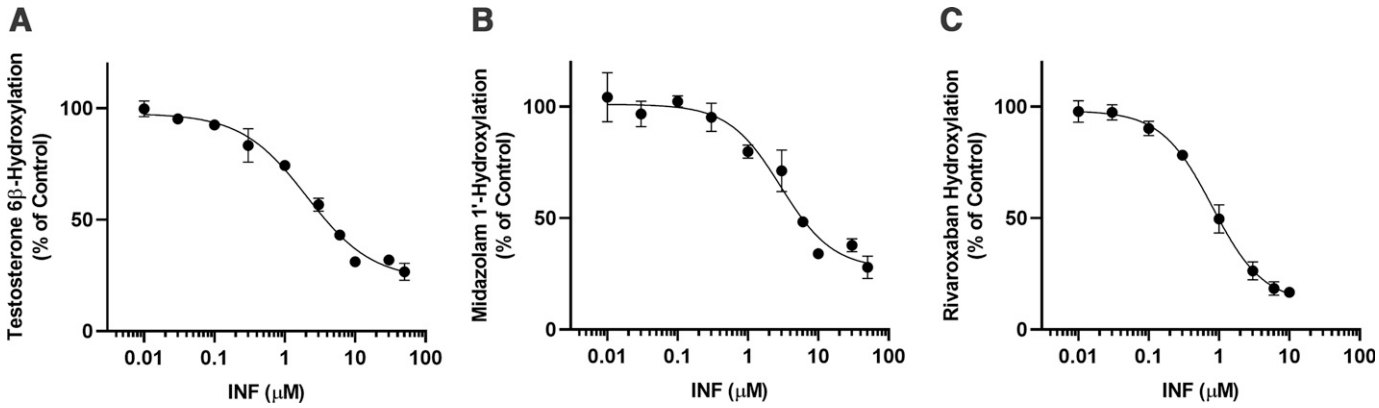

Fig. 10. Dose-response curves depicting reversible inhibition elicited by INF against CYP3A4, using (A) testosterone, (B) midazolam, and (C) rivaroxaban as probe substrates. The IC_{50} values obtained were 2.04 ± 0.29, 2.91 ± 0.54, and 0.80 ± 0.079 μM, respectively. Each point in (A–C) represents the mean and S.D. of triplicate experiments.

residue for covalent adduction (Tang et al., 2021b). Interestingly, this cysteine was determined to be substituted by a serine in CYP3A5 (i.e., Ser239) (Tang et al., 2021c). Consequently, we directed our focus on these two residues which were located in the vicinity of the F-F' loop, a region of CYP3A4 and CYP3A5 positioned directly above the orthosteric binding site (OBS) that is generally thought to function as a gate to regulate substrate access to the catalytic heme (Sevrioukova and Poulos, 2013; Benkaidali et al., 2019). Our results revealed that the top covalent docking scores obtained for INF against residue 239 of CYP3A4 (−4.7) and CYP3A5 (−5.4) were comparable (Table 3). Moreover, INF binding poses were also found to be similar in both CYP3A isoforms (Fig. 9), whereby the 2,6-dichloro-3,5-dimethoxy-phenyl moiety of INF was spatially oriented toward the F-F' loop with a minimum distance <5 Å (Table 3). Taken together, our findings suggested that INF has similar propensities to form adducts with Cys239 and Ser239 in CYP3A4 and CYP3A5, respectively.

Reversible Inhibition of CYP3A4 by INF. Finally, our MBI assays also revealed that there was a reduction in residual enzyme activity in the absence of preincubation (i.e., at zero preincubation time) (Fig. 3, A–C), thereby hinting that INF could also elicit reversible inhibition of CYP3A4. Consequently, we proceeded to establish its reversible inhibition kinetics to characterize the interactions more comprehensively between INF and CYP3A4. Our findings demonstrated that INF decreased CYP3A4-mediated testosterone 6β-hydroxylation, midazolam 1'-hydroxylation, and rivaroxaban hydroxylation in a concentration-dependent manner and yielded a sigmoidal-shaped dose-response curve with IC_{50} values of 2.04 ± 0.29, 2.91 ± 0.54, and 0.80 ± 0.08 μM, respectively (Fig. 10) (Table 4). Since INF yielded the most potent inhibition of rivaroxaban hydroxylation, we went on to determine the apparent K_i and mode of reversible inhibition using rivaroxaban as the probe substrate. Based on the nonlinear regression analysis and Lineweaver-Burk plots (Fig. 11), INF inhibited CYP3A4-mediated rivaroxaban hydroxylation noncompetitively with an apparent K_i of 0.97 ± 0.06 μM (Table 4).

TABLE 4

CYP3A4 reversible inhibition parameters for INF derived using either testosterone 6β-hydroxylation, midazolam 1'-hydroxylation, or morpholinone hydroxylation of rivaroxaban as surrogate markers of residual CYP3A activity
Data are presented as means ± S.D.

Probe Substrate	IC_{50}	K_i	Mode of Inhibition
	μM	μM	
Testosterone	2.04 ± 0.29	N.D	N.D
Midazolam	2.91 ± 0.54	N.D	N.D
Rivaroxaban	0.80 ± 0.08	0.97 ± 0.06	Noncompetitive

N.D., not determined.

Discussion

INF is a promising selective inhibitor of FGFR1–3 that is currently under clinical investigation for advanced cholangiocarcinoma and several other FGFR-linked cancers. Although its propensity to undergo bioactivation to electrophilic species was recently expounded upon, it remains obfuscated whether INF could also elicit MBI of P450, a well established consequence arising from the generation of reactive intermediates that bears profound pharmacokinetic and toxicological significance. Our findings revealed for the first time that INF is a potent noncompetitive reversible inhibitor and irreversible MBI of CYP3A4.

X-ray crystal structures of CYP3A has helped shed insights on the structural basis underpinning its ligand promiscuity (Williams et al., 2004). It is now recognized that the active site of this P450 subfamily possesses considerable bulk and plasticity which allows the simultaneous binding of multiple substrates in different modes (Kenworthy et al., 1999; Ekroos and Sjögren, 2006). As such the biochemical interactions observed with one probe substrate may not accurately reflect those obtained with another (Galetin et al., 2005; Pearson et al., 2007). Consequently, FDA guidelines recommend the use of at least two structurally disparate CYP3A substrates to evaluate whether there are any substrate- or site-dependent effects on enzyme interactions. Here, in addition to both FDA-recommended substrates, we also included rivaroxaban as a probe substrate in our assays. As rivaroxaban is increasingly being coadministered in cancer for prophylaxis and treatment of cancer-associated venous thromboembolism, its adoption as a probe substrate bears clinical significance (Short and Connors, 2014). Our findings revealed that, although INF inactivated CYP3A4 in all three probe substrates employed in our assay, there were considerable differences in their corresponding inactivation kinetic parameters (Table 1). Specifically, the k_{inact}/K_I ratio obtained with rivaroxaban was found to be ∼2.0- and 1.7-fold higher than that obtained with testosterone and midazolam, respectively. These trends in probe-substrate dependency were also recapitulated in our reversible inhibition assays, wherein INF was found to yield the lowest IC_{50} value when rivaroxaban was adopted as the probe substrate (Table 4). Taken together, our results indicated that the inhibition and inactivation of CYP3A4-mediated rivaroxaban hydroxylation by INF is expected to be more potent as compared with its FDA-recommended prototypical substrates and reiterates the importance of using a clinically relevant probe substrate

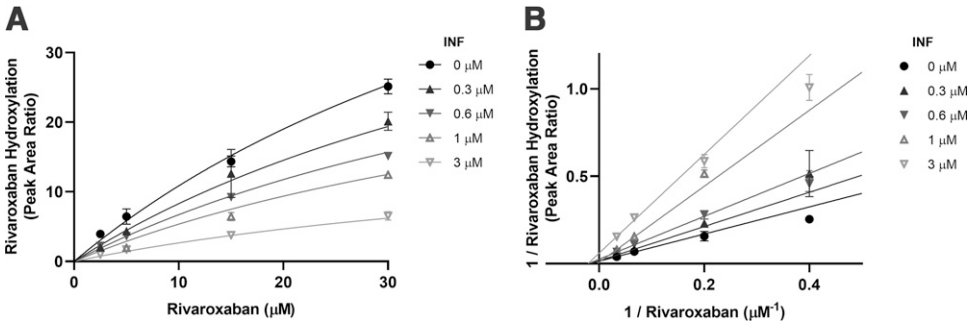

Fig. 11. Reversible inhibition of CYP3A4 by INF using rivaroxaban as the probe substrate. (A) The formation rate of hydroxylated rivaroxaban (expressed in peak area ratio) was plotted against inhibitor concentration and fitted in the Michaelis-Menten kinetic model which determined K_i to be 0.97 ± 0.06 μM. (B) Lineweaver-Burk plot revealed the mode of inhibition to be noncompetitive. Each point in (A and B) represents the mean and S.D. of triplicate experiments.

to derive accurate inhibition and/or inactivation kinetic constants for pharmacokinetic DDI studies.

The average unbound steady-state concentration of INF after a clinical dosing schedule of 125 mg daily for 3 weeks on/1 week off was previously reported to be 6.93 nM (Nogova et al., 2017). When juxtaposed with the K_I values obtained in this work, which are in the micromolar range, it is difficult to evaluate and predict the clinical consequence of the MBI of CYP3A4 by INF. However, a comparison of its k_{inact}/K_I ratio (Table 5) revealed that, although the inactivation potency of INF is eclipsed by other potent MBI (i.e., mibefradil), it was comparable to other clinically important MBI, such as clarithromycin and diltiazem, which are known to perpetrate DDIs via inactivation of CYP3A4. Taken together, it implies that a more refined estimation of INF hepatic concentration (i.e., its maximum unbound concentration within human hepatocytes) may be necessary to accurately discern its actual DDI potential. The elucidation of MBI of CYP3A4 in our study further provides a plausible mechanistic basis underpinning previous reports of INF accumulation in phase I clinical trials after chronic dosing (Nogova et al., 2017; Kelly et al., 2019). It is tempting to posit that these instances of time-dependent pharmacokinetics could arise from autoinhibition of its CYP3A4-mediated clearance pathways, although additional studies are needed to substantiate this postulation.

The efficiency of an MBI can be quantitatively assessed by its partition ratio, which is termed as the number of parent drug molecules required to completely inactivate the enzyme. Notably, compounds which possess ratios of <50 are classified as highly efficient inactivators (Lim et al., 2005). Consequently, the partition ratio of 41 suggests that INF is a relatively efficient MBI of CYP3A4. Moreover, we also demonstrated that coincubation with either testosterone or ketoconazole attenuated the rate of inactivation, implying that enzymatic inactivation by INF occurred within the active site and could be protected in the presence of an alternative substrate or direct inhibitor. Conversely, the lack of protection conferred by GSH or catalase confirmed that the putative reactive metabolite of INF inactivates the enzyme before it is liberated from the active site and ROS is not involved in enzyme inactivation.

Although our experimental findings corroborated the MBI of CYP3A4 by INF, some seeding questions pertaining to the specific nature of inactivation remains unanswered. MI complexes, which arise from the formation of dative bonds between the reactive intermediate and the heme ferrous iron, are quasi-irreversible and can be dissociated in vitro by dialysis or with potassium ferricyanide. Conversely, enzyme inactivation that proceeds via covalent adduction to either the P450 heme moiety and/or apoprotein is irreversible and cannot be mitigated by both aforementioned experimental approaches. Here, our findings demonstrated that the loss of CYP3A4 activity is irrevocable and could not be recovered after dialysis, whereas the addition of potassium ferricyanide only restored activity by a modest 4.8% which, when interpreted under the context of a published criterion (Watanabe et al., 2007); further dismisses the possibility of MI complex formation. Finally, the absence of a characteristic Soret peak and the preservation of the reduced CO binding spectrum further augmented our postulations that INF inactivates CYP3A4 via irreversible covalent adduction to the apoprotein.

As mentioned previously, the successful recapitulation of the nominal mass EPI spectral peaks in our high-resolution QTOF-MS (Supplemental Figs. 4 and 5) along with mass accuracies well below the mass tolerance threshold of 5 ppm (Table 2) gave us confidence in the predicted elemental compositions of the parent and product ions to elucidate the structure of the INF reactive intermediate. Unexpectedly, we did not manage to detect the reactive *p*-benzoquinone metabolite arising from sequential dechlorination, hydroxylation, and *O*-demethylation of the 2,6-dichloro-3,5-dimethoxy-phenyl moiety of INF that was reported by Al-Shakliah et al. (2020). Rather, the presence of the characteristic dual chlorine isotopic pattern in nominal mass measurements of the INF-derived GSH adduct further ascertained that bioactivation of INF by rhCYP3A4 did not involve dechlorination of this moiety (Supplemental Figs. 4 and 5). It should be noted that the aforementioned reported bioactivation pathway for INF was established using rat liver microsomes. Consequently, due to possible interspecies differences in P450, INF may not be liable to the same metabolic activation pathways in humans. Rather, our high-resolution MS analyses suggested that the glutathionyl moiety was alkylated directly to the INF core structure. Consequently, we proposed two alternative bioactivation pathways of INF arising from the generation

TABLE 5

Comparison of enzyme inactivation kinetic parameters between INF and several clinically important MBI of CYP3A4 using testosterone 6β-hydroxylation as a marker reaction of CYP3A activity

Compound	K_I	k_{inact}	k_{inact}/K_I	Reference
	μM	min^{-1}	$min^{-1}\ mM^{-1}$	
INF	3.26	0.027	8.4	
Clarithromycin	2.25	0.04	17.8	Polasek and Miners, 2006
Diltiazem	0.5	0.01	20.0	Ma et al., 2000
Mibefradil	2.3	0.4	173.9	Prueksaritanont et al., 1999

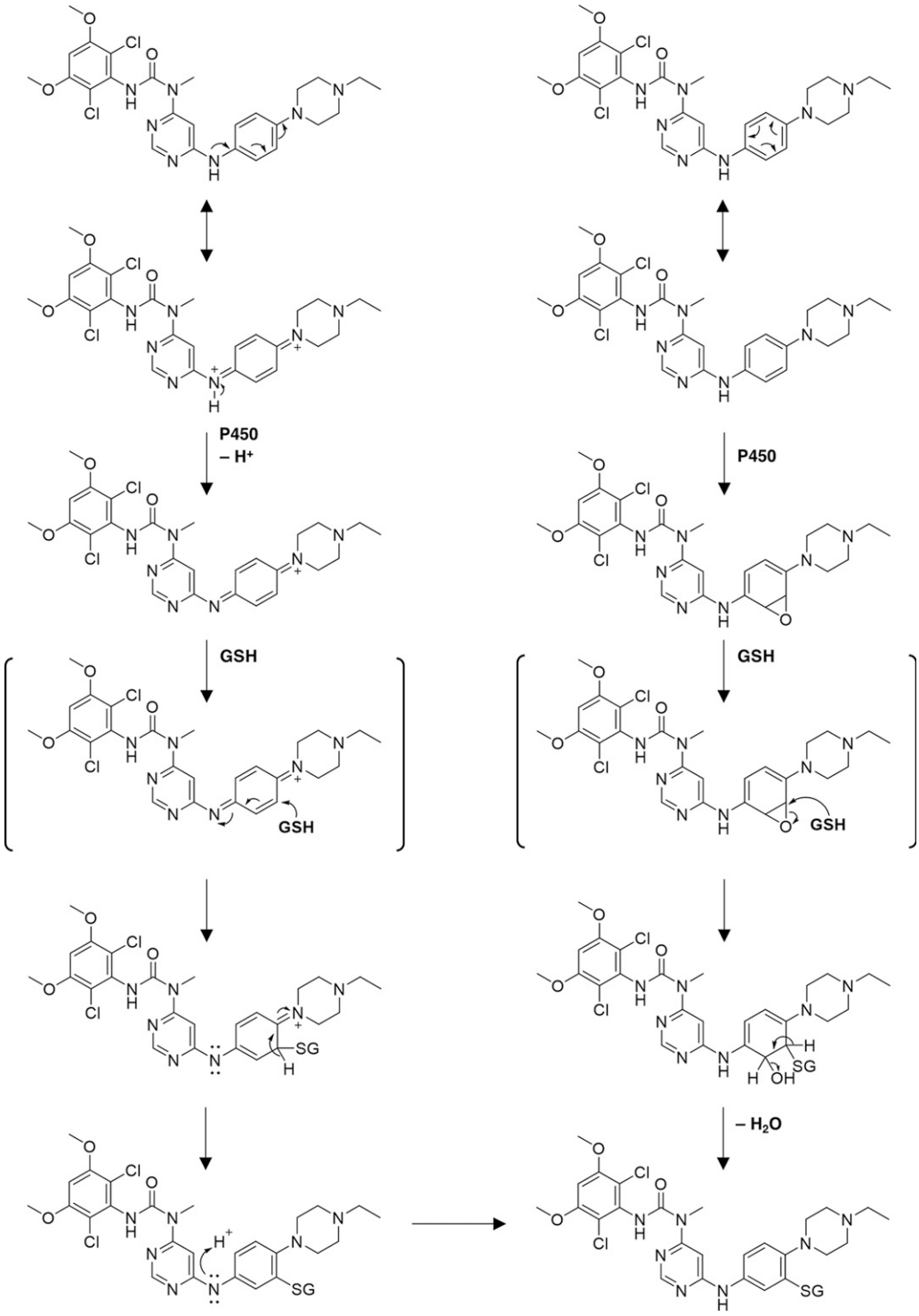

Fig. 12. Proposed bioactivation pathways of INF by CYP3A4.

of a *p*-benzoquinonediimine intermediate or an epoxide intermediate (Fig. 12). Although it is plausible that both reactive species can facilitate subsequent nucleophilic attack by GSH to form the INF-derived GSH adduct, the electron transfer pathway on the phenylenediamine moiety leading to the formation of the *p*-benzoquinonediimine intermediate may be more facile, because it is flanked by an electron deficient pyrimidine ring and a protonated (i.e., electron-withdrawing) piperazine ring which may diminish its susceptibility to P450-mediated epoxidation.

Finally, another major finding in this work is the lack of inactivation of CYP3A5 by INF. Although CYP3A5 shares ~85% sequence homology with CYP3A4, it is now generally accepted that both CYP3A isoforms have varying susceptibilities to MBI. To delineate the structural basis for this dichotomous isoform-specific inactivation profile by INF, we covalently docked the *p*-benzoquinonediimine intermediate of INF to Cys239 in CYP3A4 and Ser239 in CYP3A5. Our findings revealed that INF possesses similar propensities to form adducts with these

residues that lie adjacent to the F-F' loop. We also discovered that, unlike in CYP3A4, INF-Ser239 adducts could stabilize two distinct F-F' loop conformations in CYP3A5. Although the F-F' loop is located in proximity to the C-terminal loop in CYP3A4 and CYP3A5 ("closed" conformation) (Fig. 9, A and B), it could also be oriented further away from the C-terminal loop in CYP3A5 resulting in a wider entrance to the OBS ("open" conformation) (Fig. 9C). Taken together, it is plausible that the greater flexibility of the F-F' loop in CYP3A5 could have preserved substrate accessibility to the OBS despite similar susceptibilities to covalent alkylation by INF. These findings are concordant with our previous study involving the uricosuric agent benzbromarone which also elicited MBI of CYP3A in the same isoform-specific manner (Tang et al., 2021c) and are further corroborated by Pearson et al. (2007)'s study which underscored the key role of Cys/Ser239 in the differential inactivation of CYP3A by raloxifene.

In conclusion, our results demonstrated that INF is a potent uncompetitive inhibitor and MBI of CYP3A4. Furthermore, we also determined the nature of inactivation to be via covalent modification and elucidated the structure of the putative reactive intermediate involved in its irreversible inactivation. Given the relevance of CYP3A enzymes in drug metabolism coupled with the polymorphic expression of CYP3A5 and the emerging role of INF as a therapeutic agent for FGFR-linked cancers, further studies are warranted to better understand the pharmacogenomic and clinical implications of our findings.

Authorship Contributions

Participated in research design: Tang, Verma, Fan, Chan.

Conducted experiments: Tang, Teng, Verma, Koh.

Contributed new reagents or analytic tools: Zhou, Go.

Performed data analysis: Tang, Teng, Verma, Fan, Chan.

Wrote or contributed to the writing of the manuscript: Tang, Teng, Verma, Fan, Chan.

References

Al-Shakliah NS, Attwa MW, Kadi AA, and AlRabiah H (2020) Identification and characterization of in silico,in vivo,in vitro, and reactive metabolites of infigratinib using LC-ITMS: bioactivation pathway elucidation andin silicotoxicity studies of its metabolites. *RSC Advances* **10**:16231–16244.

Baillie TA and Davis MR (1993) Mass spectrometry in the analysis of glutathione conjugates. *Biol Mass Spectrom* **22**:319–325.

Benkaidali L, André F, Moroy G, Tangour B, Maurel F, and Petitjean M (2019) Four major channels detected in the cytochrome P450 3A4: a step toward understanding its multispecificity. *Int J Mol Sci* **20**:987.

Bjornsson TD, Callaghan JT, Einolf HJ, Fischer V, Gan L, Grimm S, Kao J, King SP, Miwa G, Ni L, et al.; Pharmaceutical Research and Manufacturers of America (PhRMA) Drug Metabolism/Clinical Pharmacology Technical Working Group; FDA Center for Drug Evaluation and Research (CDER) (2003) The conduct of in vitro and in vivo drug-drug interaction studies: a Pharmaceutical Research and Manufacturers of America (PhRMA) perspective. *Drug Metab Dispos* **31**:815–832.

Botrus G, Raman P, Oliver T, and Bekaii-Saab T (2021) Infigratinib (BGJ398): an investigational agent for the treatment of FGFR-altered intrahepatic cholangiocarcinoma. *Expert Opin Investig Drugs* **30**:309–316.

Chae YK, Ranganath K, Hammerman PS, Vaklavas C, Mohindra N, Kalyan A, Matsangou M, Costa R, Carneiro B, Villaflor VM, et al. (2017) Inhibition of the fibroblast growth factor receptor (FGFR) pathway: the current landscape and barriers to clinical application. *Oncotarget* **8**:16052–16074.

Chan ECY, New LS, Chua TB, Yap CW, Ho HK, and Nelson SD (2012) Interaction of lapatinib with cytochrome P450 3A5. *Drug Metab Dispos* **40**:1414–1422.

Dieckhaus CM, Fernández-Metzler CL, King R, Krolikowski PH, and Baillie TA (2005) Negative ion tandem mass spectrometry for the detection of glutathione conjugates. *Chem Res Toxicol* **18**:630–638.

Dienstmann R, Rodon J, Prat A, Perez-Garcia J, Adamo B, Felip E, Cortes J, Iafrate AJ, Nuciforo P, and Tabernero J (2014) Genomic aberrations in the FGFR pathway: opportunities for targeted therapies in solid tumors. *Ann Oncol* **25**:552–563.

Ekroos M and Sjögren T (2006) Structural basis for ligand promiscuity in cytochrome P450 3A4. *Proc Natl Acad Sci USA* **103**:13682–13687.

Galetin A, Ito K, Hallifax D, and Houston JB (2005) CYP3A4 substrate selection and substitution in the prediction of potential drug-drug interactions. *J Pharmacol Exp Ther* **314**:180–190.

Guengerich FP (2001) Common and uncommon cytochrome P450 reactions related to metabolism and chemical toxicity. *Chem Res Toxicol* **14**:611–650.

Haugsten EM, Wiedlocha A, Olsnes S, and Wesche J (2010) Roles of fibroblast growth factor receptors in carcinogenesis. *Mol Cancer Res* **8**:1439–1452.

Ho HK, Chan JCY, Hardy KD, and Chan ECY (2015) Mechanism-based inactivation of CYP450 enzymes: a case study of lapatinib. *Drug Metab Rev* **47**:21–28.

Hong Y, Chia YMF, Yeo RH, Venkatesan G, Koh SK, Chai CLL, Zhou L, Kojodjojo P, and Chan ECY (2016) Inactivation of human cytochrome P450 3A4 and 3A5 by dronedarone and n-desbutyl dronedarone. *Mol Pharmacol* **89**:1–13.

Hoy SM (2020) Pemigatinib: first approval. *Drugs* **80**:923–929.

Javle M, Lowery M, Shroff RT, Weiss KH, Springfeld C, Borad MJ, Ramanathan RK, Goyal L, Sadeghi S, Macarulla T, et al. (2018) Phase II study of BGJ398 in patients with FGFR-altered advanced cholangiocarcinoma. *J Clin Oncol* **36**:276–282.

Karkhanis A, Lam HY, Venkatesan G, Koh SK, Chai CLL, Zhou L, Hong Y, Kojodjojo P, and Chan ECY (2016) Multiple modes of inhibition of human cytochrome P450 2J2 by dronedarone, amiodarone and their active metabolites. *Biochem Pharmacol* **107**:67–80.

Kelly CM, Shoushtari AN, Qin LX, D'Angelo SP, Dickson MA, Gounder MM, Keohan ML, Mcfadyen C, Sjoberg A, Singer S, et al. (2019) A phase Ib study of BGJ398, a pan-FGFR kinase inhibitor in combination with imatinib in patients with advanced gastrointestinal stromal tumor. *Invest New Drugs* **37**:282–290.

Kenworthy KE, Bloomer JC, Clarke SE, and Houston JB (1999) CYP3A4 drug interactions: correlation of 10 in vitro probe substrates. *Br J Clin Pharmacol* **48**:716–727.

Kim S, Chen J, Cheng T, Gindulyte A, He J, He S, Li Q, Shoemaker BA, Thiessen PA, Yu B, et al. (2019) PubChem 2019 update: improved access to chemical data. *Nucleic Acids Res* **47** (D1):D1102–D1109.

Kitz R and Wilson IB (1962) Esters of methanesulfonic acid as irreversible inhibitors of acetylcholinesterase. *J Biol Chem* **237**:3245–3249.

Lim HK, Duczak Jr N, Brougham L, Elliot M, Patel K, and Chan K (2005) Automated screening with confirmation of mechanism-based inactivation of CYP3A4, CYP2C9, CYP2C19, CYP2D6, and CYP1A2 in pooled human liver microsomes. *Drug Metab Dispos* **33**:1211–1219.

Ma B, Prueksaritanont T, and Lin JH (2000) Drug interactions with calcium channel blockers: possible involvement of metabolite-intermediate complexation with CYP3A. *Drug Metab Dispos* **28**:125–130.

Markham A (2019) Erdafitinib: first global approval. *Drugs* **79**:1017–1021.

Masubuchi Y and Horie T (2007) Toxicological significance of mechanism-based inactivation of cytochrome p450 enzymes by drugs. *Crit Rev Toxicol* **37**:389–412.

Mosconi S, Beretta GD, Labianca R, Zampino MG, Gatta G, and Heinemann V (2009) Cholangiocarcinoma. *Crit Rev Oncol Hematol* **69**:259–270.

Nogova L, Sequist LV, Perez Garcia JM, Andre F, Delord JP, Hidalgo M, Schellens JHM, Cassier PA, Camidge DR, Schuler M, et al. (2017) Evaluation of BGJ398, a Fibroblast growth factor receptor 1-3 kinase inhibitor, in patientswith advanced solid tumors harboring genetic alterations in fibroblast growth factor receptors: results of a global phase I, dose-escalation and dose-expansion stud. *J Clin Oncol* **35**:157–165.

Omura T and Sato R (1964) The carbon monoxide-binding pigment of liver microsomes. I. evidence. *J Biol Chem* **239**:2370–2378.

Pearson JT, Wahlstrom JL, Dickmann LJ, Kumar S, Halpert JR, Wienkers LC, Foti RS, and Rock DA (2007) Differential time-dependent inactivation of P450 3A4 and P450 3A5 by raloxifene: a key role for C239 in quenching reactive intermediates. *Chem Res Toxicol* **20**:1778–1786.

Polasek TM and Miners JO (2006) Quantitative prediction of macrolide drug-drug interaction potential from in vitro studies using testosterone as the human cytochrome P4503A substrate. *Eur J Clin Pharmacol* **62**:203–208.

Polasek TM and Miners JO (2008) Time-dependent inhibition of human drug metabolizing cytochromes P450 by tricyclic antidepressants. *Br J Clin Pharmacol* **65**:87–97.

Prueksaritanont T, Ma B, Tang C, Meng Y, Assang C, Lu P, Reider PJ, Lin JH, and Baillie TA (1999) Metabolic interactions between mibefradil and HMG-CoA reductase inhibitors: an in vitro investigation with human liver preparations. *Br J Clin Pharmacol* **47**:291–298.

Reyes M, Belcher V, Hormel K, Chung D, Guptha S, Zamora C, Atiee G, Roupe K, Zhang W, Moran S, et al. (2020) PII-053 drug interaction potential of infigratinib (BGJ398), a potent and selective FGFR1–3 inhibitor, in healthy volunteers (HV): pharmacokinetics (PK) and safety. *Clin Pharmacol Ther* **107**:S49–S50.

Sevrioukova IF and Poulos TL (2013) Understanding the mechanism of cytochrome P450 3A4: recent advances and remaining problems. *Dalton Trans* **42**:3116–3126.

Short NJ and Connors JM (2014) New oral anticoagulants and the cancer patient. *Oncologist* **19**:82–93.

Silverman RB (1995) Mechanism-based enzyme inactivators. *Methods Enzymol* **249**:240–283.

Stephens C, Andrade RJ, and Lucena MI (2014) Mechanisms of drug-induced liver injury. *Curr Opin Allergy Clin Immunol* **14**:286–292.

Tang LWT, Teng JW, Koh SK, Zhou L, Go ML, and Chan ECY (2021a) Mechanism-based inactivation of cytochrome P450 3A4 and 3A5 by the fibroblast growth factor receptor inhibitor Erdafitinib. *Chem Res Toxicol* **34**:1800–1813.

Tang LWT, Verma RK, Fan H, and Chan ECY (2021b) Mechanism-based inactivation of cytochrome P450 3A4 by Benzbromarone. *Mol Pharmacol* **99**:266–276.

Tang LWT, Verma RK, Yong RP, Li X, Wang L, Lin Q, Fan H, and Chan ECY (2021c) Differential reversible and irreversible interactions between Benzbromarone and human cytochrome P450s 3A4 and 3A5. *Mol Pharmacol* DOI: https://doi.org/10.1124/molpharm.121.000256 [published ahead of print].

Teng WC, Oh JW, New LS, Wahlin MD, Nelson SD, Ho HK, and Chan ECY (2010) Mechanism-based inactivation of cytochrome P450 3A4 by lapatinib. *Mol Pharmacol* **78**:693–703.

Turner N and Grose R (2010) Fibroblast growth factor signalling: from development to cancer. *Nat Rev Cancer* **10**:116–129.

Watanabe A, Nakamura K, Okudaira N, Okazaki O, and Sudo K (2007) Risk assessment for drug-drug interaction caused by metabolism-based inhibition of CYP3A using automated in vitro assay systems and its application in the early drug discovery process. *Drug Metab Dispos* **35**:1232–1238.

Williams PA, Cosme J, Vinkovic DM, Ward A, Angove HC, Day PJ, Vonrhein C, Tickle IJ, and Jhoti H (2004) Crystal structures of human cytochrome P450 3A4 bound to metyrapone and progesterone. *Science* **305**:683–686.

Zanger UM and Schwab M (2013) Cytochrome P450 enzymes in drug metabolism: regulation of gene expression, enzyme activities, and impact of genetic variation. *Pharmacol Ther* **138**:103–141.

Zanger UM, Turpeinen M, Klein K, and Schwab M (2008) Functional pharmacogenetics/genomics of human cytochromes P450 involved in drug biotransformation. *Anal Bioanal Chem* **392**:1093–1108.

Zhu K, Borrelli KW, Greenwood JR, Day T, Abel R, Farid RS, and Harder E (2014) Docking covalent inhibitors: a parameter free approach to pose prediction and scoring. *J Chem Inf Model* **54**:1932–1940.

Address Correspondence to: Professor Eric Chun Yong Chan, Department of Pharmacy, National University of Singapore, 18 Science DR. 4, Singapore 117543. E-mail: phaccye@nus.edu.sg